High-Speed Photographic Study of Wave Propagation and Impact Damage in Transparent Aluminum Oxynitride (AlON)
Final Report

Report E 08/06

Item No. 0003
Research period: 07/2004 – 07/2005
Contract No. N62558-04-P-6031

Contractor:
Fraunhofer-Gesellschaft zur Förderung der angewandten Forschung e.V.
Hansastraße 27c, D-80686 München, Germany

The research reported in this document has been made possible through the support and sponsorship of the U.S. Government through its European Research Office of the U.S. Army. This report is intended only for the internal management use of the Contractor and the U.S. Government.

Prepared by:
E. Straßburger

Management:
E. Straßburger

February 2006
Efringen-Kirchen,
Germany

High-Speed Photographic Study of Wave Propagation and Impact Damage in Transparent Aluminum Oxynitride (AlON)
Final Report

Report E 08/06

Ordering Customer   U.S. ARL – European Research Office
                              Naval Regional Contracting Center, Det. London
Contract Number   N62558-04-P-6031
Classification   U

Preparation   _____
and Management: E. Straßburger
                           Group Manager – Light Armour

                           _____
                           Dr. M. Salk
                           Head of Department – Experimental Ballistics

                           _____
                           Prof. Dr. K. Thoma
                           Director of Ernst-Mach-Institut

Table of Contents

1   Introduction

When a high-speed projectile hits a brittle material like glass or ceramic severe fragmentation can be observed, preceding the penetration of the projectile. Several types of glass [1,2] ceramic [3] and a glass-ceramic [4] have already been studied at EMI by means of the Edge-on Impact test.

Fused silica and AlON are materials being considered for a variety of transparent armor, sensor window and radome applications. AlON is a polycrystalline ceramic that fulfills the requirements of transparency and requisite mechanical properties for transparent armor against armor piercing ammunition. [5]. AlON has a cubic crystal structure (Fd3m) that can be processed to transparency in a polycrystalline microstructure. It differs from glasses which do not have any periodic crystalline order, but is akin to polycrystalline opaque ceramics such as aluminum oxide.

In the current study, two different optical configurations were employed. A regular transmitted light shadowgraph set-up was used to observe wave and damage propagation and a modified configuration, where the specimens were placed between crossed polarizers and the photo-elastic effect was utilized to visualize the stress waves. Pairs of impact tests at approximately equivalent velocities were carried out in transmitted plane (shadowgraphs) and crossed polarized light. AlON and fused silica specimens were impacted using solid cylinder steel projectiles with velocities ranging from 270 to 925 m/s. The nucleation of crack centers was observed ahead of the apparent fracture front, growing from the impacted edge of the specimens. A comparison of the shadowgraphs to photographs recorded in a reflected light configuration with a coated AlON specimen at the same impact conditions, indicated fracture nucleation in the interior of the ceramic.

2 Statement of work

2.1 Results with Fused Silica

The optical configurations and the experimental results have been described and discussed in detail in the 1st and 2nd Interim Report [6, 7] and in a publication at the 22nd International Symposium on Ballistics [8]. Therefore, only a short summary and discussion of the results is given here.

The tests were performed as one single shot at 125 m/s and three pairs of shots at nominal impact velocities of 150 m/s, 250 m/s and 350 m/s. With each pair of shots one test was conducted in the regular shadowgraph configuration and the other test with additional crossed polarizers. The test matrix is given in Table 1. The last two columns list the time intervals between the photographs. In each test 20 photographs were recorded.

Table 1: Tests with fused silica.

Test No.	Impact Vel. [m/s]	Set-up	Time Intervals	
14885	125	No Polarizers	1-16: 1 µs	16-20: 2 µs
14880	155	No Polarizers	1-16: 1 µs	16-20: 2 µs
14881	≈150	Crossed Polarizers	1-16: 1 µs	16-20: 2 µs
14891	≈260	No Polarizers	1-20: 1 µs	
14893	262	Crossed Polarizers	1-20: 1 µs	
14877	350	Crossed Polarizers	1-13: 1 µs	13-20: 2 µs
14878	348	No Polarizers	1-13: 1 µs	13-20: 2 µs

The velocities specified with tests number 14881 and 14891 were estimated on the basis of the thickness of the aluminium diaphragm used in the gas gun. Due to the high reproducibility observed it can be assumed that the impact velocity in those tests was within a range of ± 10 m/s around the impact velocity of the other test with the same diaphragm thickness.

Figure 1 shows eight shadowgraphs and the corresponding crossed polarizers photographs of two tests conducted at 350 m/s. Note that damage appears dark on the shadowgraphs and the zones with stress birefringence are exhibited as bright zones in the crossed polarizers photographs. The

shadowgraphs and crossed polarizers photographs are aligned one below the other, allowing for a direct comparison. The time of each pair of photographs is denoted in the crossed polarizers photographs. The moment of impact (t = 0 µs) was determined by means of a short circuit between two trigger foils at the impact edge of the specimens, generated by the projectile.
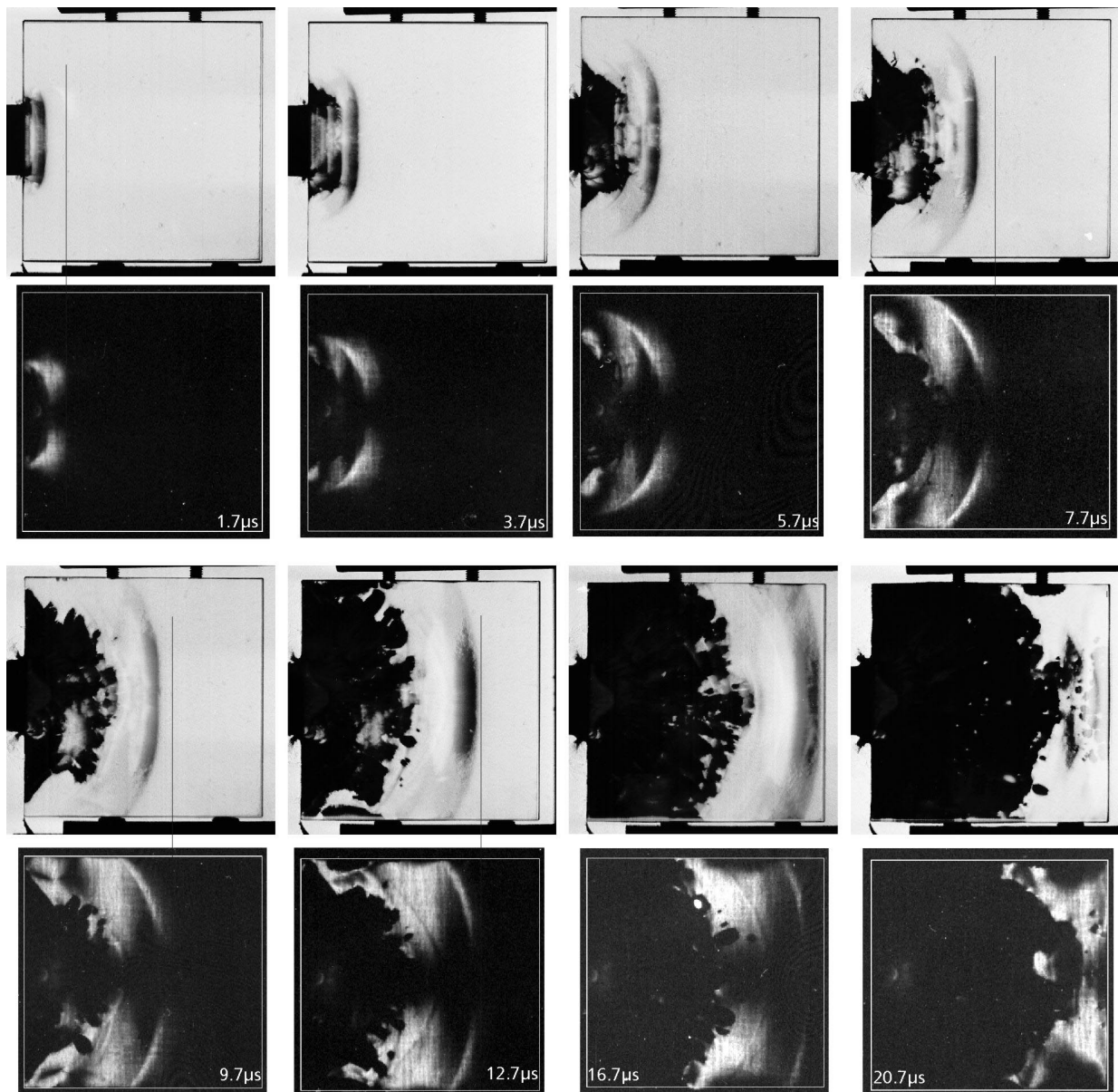

Fig. 1:   Test No. 14877-78: Selection of 8 shadowgraphs and corresponding crossed polarizers photographs from impact on fused silica at 350 m/s.

On the shadowgraphs it can be seen that damage starts first where the edge of the projectile impacts the specimen. Triangularly shaped damage zones spread towards the upper and lower edge of the specimen. The photographs also show the rapid growth of separated, damage zones ahead of the projectile, seemingly due to crack nucleation and growth apparently created by the stress wave interaction with pre-existing processing defects or structural inhomogenieties in the fused silica. The stress waves itself exhibits a relatively plane front in the centre and a curved shape outwards.

Unlike the shadowgraphs, in the crossed polarizers pictures an approximately semicircular wave front can be recognized, which is further advanced compared to the front visible in the shadowgraphs at the same time. However, the stress wave is not as clearly defined (especially in the center) as the actual damage front in the shadowgraphs. The vertical lines in some pairs of photographs indicate the position of the wave front in the crossed polarizers view.

The photographs taken with the two different recording techniques reveal different processes. In the crossed polarizers arrangement those zones of the specimen are visible, where the stresses are high enough to cause birefringence, so that enough light passes through in order to expose the film. Thus, in the crossed polarizers configuration basically the stress field is visualized. In the regular shadowgraph arrangement those zones of the specimen appear dark, where the material is either damaged or fractured and, therefore, blocking light transmission or where the light is absorbed more strongly due to a pressure induced change in refractive index.

The quantitative results for wave and damage/fracture velocities are presented in Table 2. Considering the wave front velocities, determined with both optical set-ups, the same observation was made at all impact velocities: the wave front was further advanced in the crossed polarizers view (see Fig. 1), but the wave velocity was lower compared to the waves observed in the shadowgraphs (see Table 2).

Table 2: Compilation of measured wave, crack and damage velocities.

Impact Velocity v_P		[m/s]	150	260	350
Long. Wave Speed	Shadowgraphs	[m/s]	5975	6076	5823
Long. Wave Speed	Crossed Polarizers	[m/s]	5814	5796	5491
Trans. Wave Speed	Shadowgraphs	[m/s]	---	3500	3670
Crack Velocity	Shadowgraphs	[m/s]	2234	2149	2120
Damage Velocity	Shadowgraphs	[m/s]	5641	5728	5121

The correct interpretation of the results requires an understanding of the dependence of the deflection of light on the loading of the specimens. In order to distinguish between light deflections caused by surface deformation and deflections caused by changes of the refractive index a reflection Schlieren set-up was devised at EMI by H. Vollkommer [9] in which glass plates were loaded at one edge by a wire explosion. The upper half of the glass specimen was coated with a reflective layer at the front surface and the lower half was similarly coated at the back surface. The tests demonstrated that in the zone of the longitudinal waves, surface deformation is irrelevant, while the refractive index changes dominate, whereas behind the transversal wave front, light deflection through surface deformation is the dominant effect. In a shadowgraph image the light intensity depends on the second spatial derivative $\partial^2 n/\partial x^2$ of the refractive index [10]. When the photo-elastic behavior of a material is known the amplitudes of the pressure pulses can be determined. Beinert [11] developed a method to calibrate a Schlieren set-up and measured the amplitude and shape of pressure pulses in glass plates generated by wire explosions at one edge.

In the present study neither the shapes of the pressure pulses are known, nor whether the pulse shapes change during propagation in the edge-on impacted plates. However, the amplitude and shape of pressure pulses determine where the change in density, and therefore in the refractive index, is strong enough to cause a deflection of light that can be detected with the optical set-up used. The sequence of events along the pressure pulse/wave may be assumed to be as follows: rising pressure induces a density increase causing a linear change in refractive index until a pressure is reached when the glass becomes birefringent. The glass continues to densify until the structure collapses and irreversible damage begins to form. If the pressure pulse amplitude and shape did not change it could be expected that the same propagation velocity were observed with the shadowgraph and the crossed polarizers arrangement. Due to the specimen geometry a sequence of pressure pulses is formed, caused by partial reflections of the first pulse at the surfaces and by the reflection of the transversal waves which are drawn along the surfaces. This phenomenon was also observed and described with the Edge-On Impact tests in different types of glass [12]. Beinert demonstrated that energy is continuously transferred from the first pressure pulse to the next one and therefore the amplitude decreases steadily. The decreasing amplitude together with the shape of the pulses could explain the seemingly different velocities, since it can be assumed that the sensitivity of the two optical set-ups is different. Analysis of these results and interpretations are still on going.

2.2   Results with AlON

AlON specimens of thickness 10 mm and two specimens of 25 mm thickness with lateral dimensions 100 mm x 100 mm were delivered for impact testing to EMI. The flat surfaces of the specimens and all the edges were polished in order to enable observation with high-speed cameras from all directions. However, it turned out that due to light scattering it was not possible to get a clear view through a thickness of 100 mm (from edge to edge). Therefore, the pictures recorded with the top view camera did not show any details of the damage progression inside the specimens. Those pictures could be used to control the impact position of the projectile, especially in the tests where the powder gun was used, so that the projectile hit the specimen after a free flight over a distance of 170 cm.

The tests with AlON were conducted in the velocity range from 250 m/s to 950 m/s. The test matrix is given in Table 3. As with the fused silica, the tests with AlON were performed in pairs of shots at the same nominal velocity, whereas one test was conducted in the shadowgraph configuration and the other test with the crossed polarizers set-up. The nominal impact velocities were 270 m/s, 380 m/s, 600 m/s and 850 m/s.

Table 3: Test matrix with AlON.

Test No.	Impact Vel. [m/s]	Set-up	Cameras	Time Intervals	
14894	278	No Polarizers	2	1-20: 0.5µs	
14895	270	Cr. Polarizers	2	1-20: 0.5µs	
14897	381	No Polarizers	2	1-18: 0.5µs	18-20: 1µs
14898	368	Cr. Polarizers	2	1-18: 0.5µs	18-20: 1µs
14906	820	No Polarizers	2	1-18: 0.5µs	18-20: 1µs
14907	925	Cr. Polarizers	2	1-18: 0.5µs	18-20: 1µs
14908	588	No Polarizers	2	1-18: 0.5µs	18-20: 1µs
14909	664	Cr. Polarizers	2	1-18: 0.5µs	18-20: 1µs
14923	390	No Polarizers Inhomog. Spec.*	2	1-16: 0.5µs	16-20: 1µs
14924	385	No Polarizers Spec. with defect	2	1-16: 0.5µs	16-20: 1µs
14925	385	No Polarizers 25 mm Specimen	2	1-16: 0.5µs	16-20: 1µs
14940	397	No polarizers Reflected light	1	1-20: 0.5µs	

* Inhomogeneous Specimen

The results with test numbers 14894, -895, -897, -898 and 14940 were described and analyzed in the 2nd Interim Report and partly published at the

22nd International Symposium on Ballistics [13]. Therefore, this report focuses on the analysis of the EOI-tests at high impact velocities (14906 – 14909), tests with specimens with inhomogenieties (14923, 14924) and a test with a specimen of 25 mm thickness.

2.2.1 Tests at high impact velocities

In order to achieve impact velocities between 400 m/s and 950 m/s a 30 mm powder gun with a rifled barrel had to be used for the acceleration of the projectiles. Due to the muzzle flash and the fumes the specimens could not be placed in a short distance to the muzzle. In those cases the distance between the muzzle and the specimens was 170 cm. The use of the powder gun and the type of projectile (steel cylinder with steel guidance band for transfer of twist) caused a relatively high scatter in the muzzle velocity.

Tests No. 14906/ 14907; v_P = 820/ 925 m/s

Figure 2 shows a selection of four shadowgraphs and the corresponding crossed polarizers photographs at impact velocities of 820 m/s and 925 m/s, respectively.
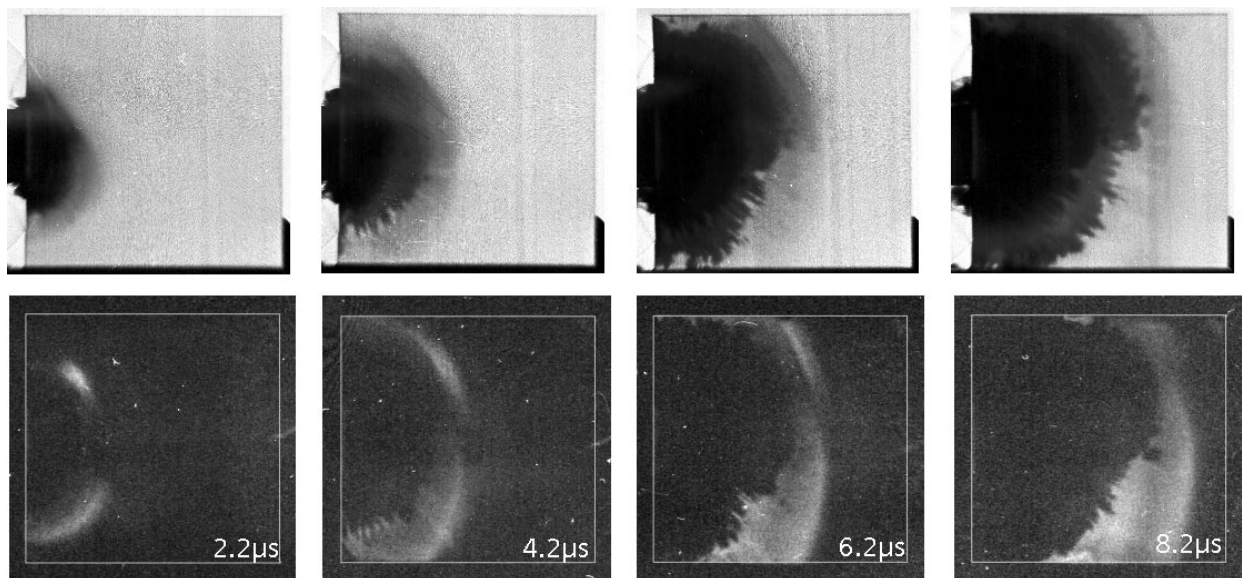

Fig. 2: Selection of four shadowgraphs and corresponding crossed polarizers photographs from impact on AlON.

The series of high-speed photographs shows rapidly growing darkened to opaque regions, which reflect changes in the optical transmission due to pressure induced refractive index changes, damaged and fractured zones within the specimen. In addition, the nucleation of crack centres ahead of the crack front is clearly visible 6.2 and 8.2 µs after impact. In contrast to the shadowgraphs, where a wave front is not clearly discernable, the crossed polarizers configuration reveals an approximately semicircular wave front which is a little further advanced compared to the damage front visible in the shadowgraphs at the same time. The complete series of photographs are shown in the appendix, Figures A1 and A2.

Figure 3 illustrates path-time data of wave and damage/fracture propagation for the two tests. The data of the wave propagation, determined from the crossed polarizers test, are represented by the red filled circles. Two linear regions with different slopes can be distinguished.
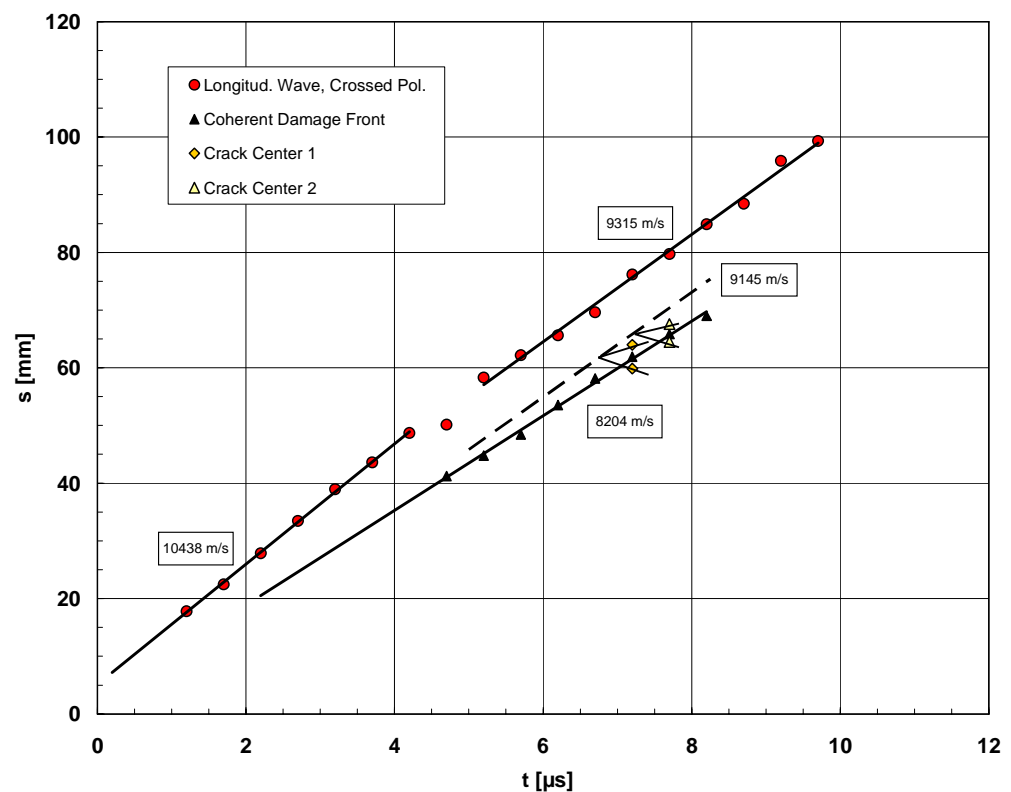

Fig. 3:   Path-time data of wave and fracture propagation at impact velocities 820 m/s and 925 m/s.

Linear regression of the data from 1.2 μs to 4.2 μs yields an average wave speed of 10438 m/s, which approximately corresponds to the longitudinal wave speed of 10300 m/s determined by means of ultrasonic wave measurements. Between 4 and 5 μs after impact a deceleration of the wave speed seems to occur, whereas after 5 μs a linear section is observed again. Linear regression of that part of the data yields an average wave speed of 9315 m/s. The phenomenon of an apparent deceleration, followed by another linear section was already observed more distinctly in AlON with the damage front in the tests at lower impact velocities [7]. This optical effect was denoted birefringence shift and was attributed to the stress induced birefringence. However, it is not clear yet, why a change in the average wave speed is observed. The complete series of high-speed photographs from the crossed polarizers set-up (see Fig. A2) shows, that during the first 4.2 μs the stress wave front, which appears bright on the photographs, is not visible in the centre. From picture no. 9 (4.7 μ) the stress wave front forms a coherent bright zone. This suggests a correlation between the appearance of the stress wave front and the measured velocity. In the tests at lower impact velocities a coherent stress wave front was visible in nearly all the photographs and split-up in sections with different slopes was not observed. The major difference between the high and low velocity tests, with respect to the impact conditions, is the accuracy. The projectile is still guided in the barrel of the gas gun for impact velocities below 450 m/s, whereas the free flight distance of 170 cm at high impact velocities allows yawing of the projectile and an off-set from the axis through the gun barrel and the specimen. This is illustrated in Figure 4, which shows a top view of the impacted specimen from tests no. 14906 and 14909.
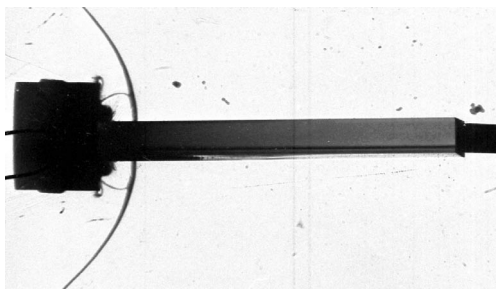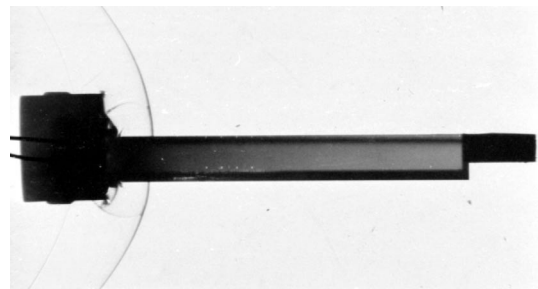

Fig. 4a: Test No. 14906, Top view, t = 0.7 μs. Fig. 4b: Test No. 14909, Top view, t = 0.7 μs.

As the side view photographs of test no. 14906 show (Fig. A1) yaw of the projectile in the vertical plane (parallel to the 100 mm square surfaces) results in an asymmetric formation of the damage front. Yaw in the horizontal plane, perpendicular to the 100 mm square surfaces, also strongly affects wave propagation in the specimen. Since the thickness of the specimen is only 10 mm, yaw of the projectile can cause a multitude of reflections and

superposition of waves, which can affect the stress states and the visibility of the stress wave front.

Considering the velocity of the coherent damage front, which grew at an average velocity of 8204 m/s, no significant differences to the low velocity impact tests were observed. The number of crack centers ahead of the coherent fracture front was not significantly higher with the high impact velocity. The damage velocity, determined by linear regression through the nucleation sites of the crack centers, was 9145 m/s (dashed line Fig. 3).

Tests No. 14908/ 14909; v_P = 588/ 664 m/s

Figure 5 shows a selection of four shadowgraphs and the corresponding crossed polarizers photographs at impact velocities of 588 m/s and 664 m/s, respectively. The complete series of photographs are shown in the Appendix, Figures A3 and A4.
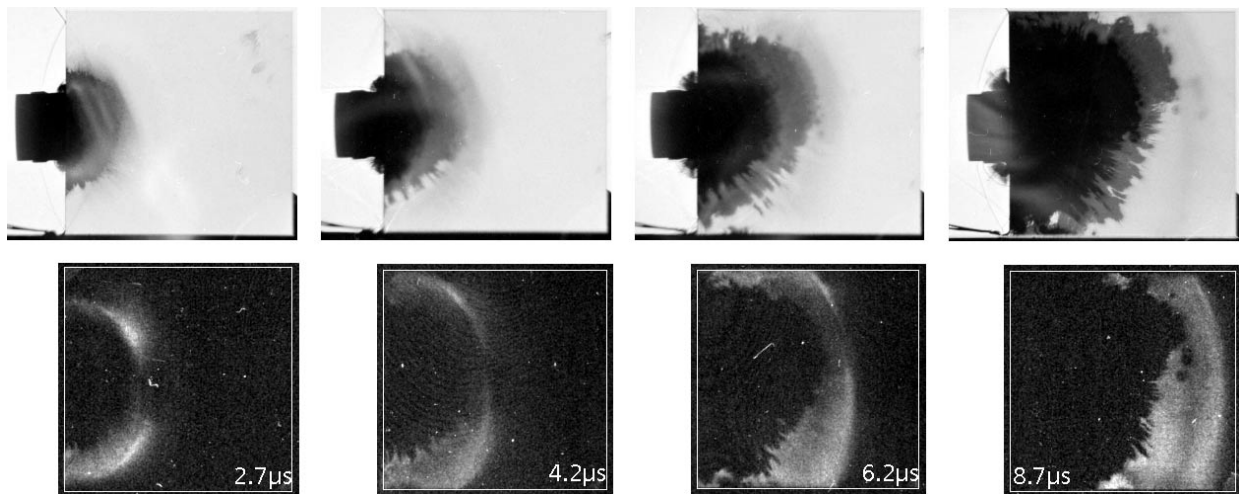

2.7μs 4.2μs 6.2μs 8.7μs

Fig. 5:   Selection of four shadowgraphs and corresponding crossed polarizers photographs from impact on AlON.

Considering fracture formation, the high-speed photographs basically show the same characteristics as observed at other impact velocities. The positions of the wave front, fracture front and the crack centers are plotted versus time in Figure 6. The average velocity of the coherent fracture front was 8413 m/s. The development of five crack centers could be observed and linear regression through the nucleation points yields a damage velocity of 8976 m/s.
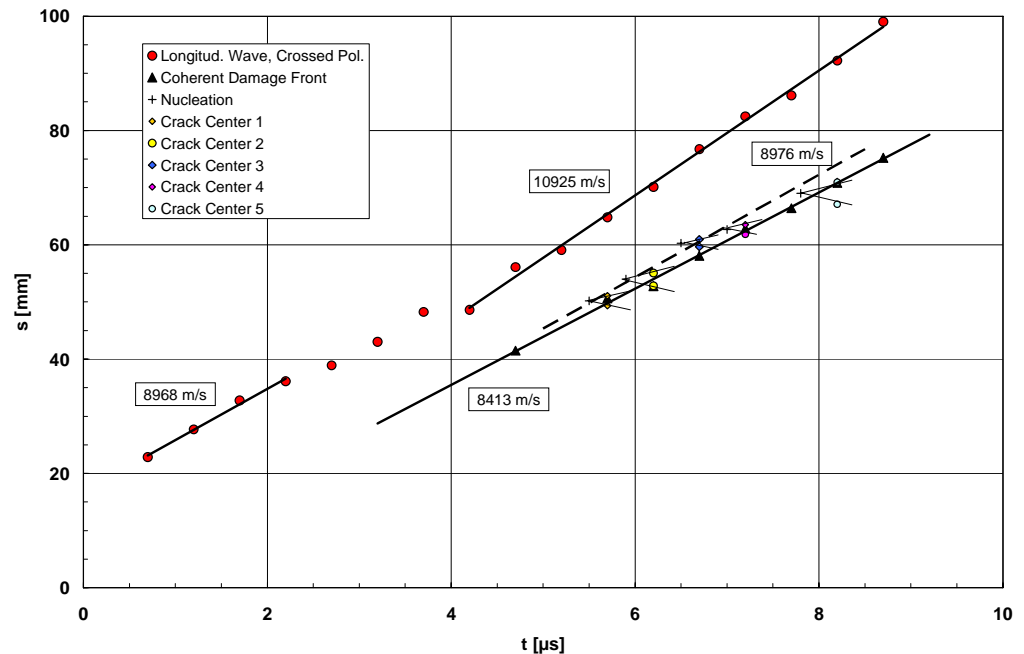
Fig. 6:   Path-time data of wave and fracture propagation at impact velocities
            588 m/s and 664 m/s.

As observed in test no. 14907, sections with different slopes (wave velocities)
can be distinguished. The most obvious change is again observed at about 4 µs.
However, in this test a lower wave propagation velocity (8968 m/s) is observed
before 4 µs and a higher velocity (10925 m/s) after 4 µs. The most striking
feature of the wave position data during the first microseconds is the high off-
set. In order to reach the measured positions the wave velocity would have to
be unrealistically high during the first microsecond after impact. Therefore, it
appears more plausible that the off-set is either due to birefringence shift or to
a delayed trigger signal, caused by a slightly inclined impact of the projectile as
can be seen from the top view photograph in Figure 4b.

2.2.2   Tests with inhomogeneous specimens

An optical inspection of the specimens between crossed polarizers on a light
box revealed inhomogenieties of the material in some cases. Figure 7 shows a
specimen of 10 mm thickness on a light box with one sheet polarizer under the
specimen (left) and between two crossed polarizers (right). The picture with the
crossed polarizers reveals four zones where light passes through the specimen,
arranged symmetrically like four petals of a blossom, directed towards the

corners of the AlON specimen. This phenomenon was observed clearly with both specimens of 25 mm thickness; with two specimens of 10 mm thickness and it could be seen faintly with a few other specimens. It is assumed that it is connected to internal stresses due to an inhomogeneous temperature distribution in the furnace during sintering and cooling.
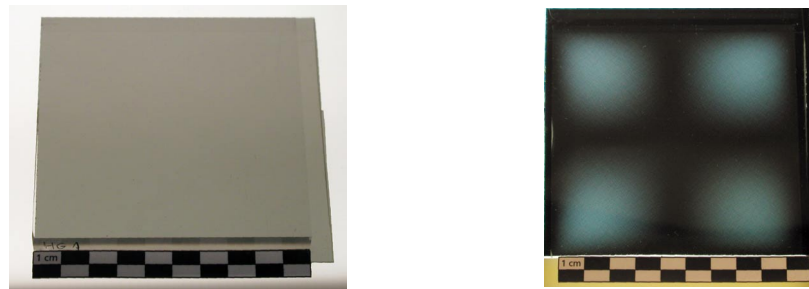

Fig. 7:   Specimen with inhomogenieties on a light box with one polarizer beneath (left) and between crossed polarizers (right).

One specimen with inhomogenieties as described above was tested at 390 m/s in a shadowgraph configuration. Figure 8 shows a selection of eight photographs from this test. The complete series of photographs is presented in Figure A5 of the Appendix.
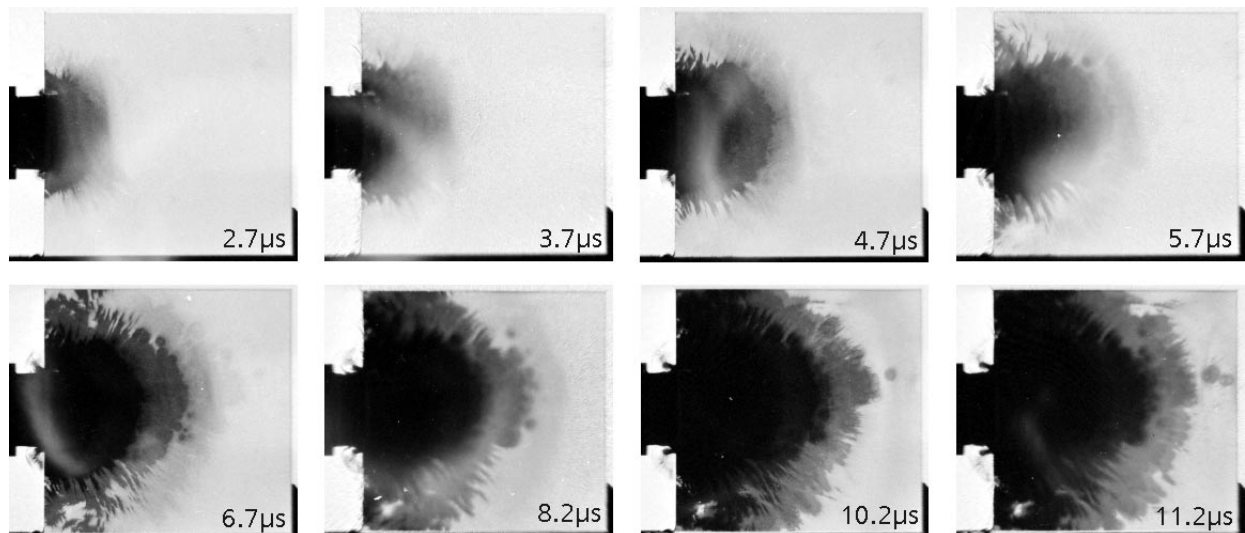

Fig. 8:   Selection of eight shadowgraphs from impact on inhomogeneous AlON specimen, Test No. 14923, v_p = 390 m/s.

The photographs illustrate that no influence of the inhomogenieties on fracture formation was found. The same phenomena and a fracture front velocity of the same order of magnitude as in other tests at similar conditions were observed. This is demonstrated by the path-time histories plotted in Figure 9. The front that was observed during the first four microseconds propagated at an average velocity of 10589 m/s, which corresponds to the longitudinal wave velocity. The average speed of the coherent fracture front was 8934 m/s. Considering the crack centers ahead of the coherent fracture front, a damage velocity of 9054 m/s could be determined.
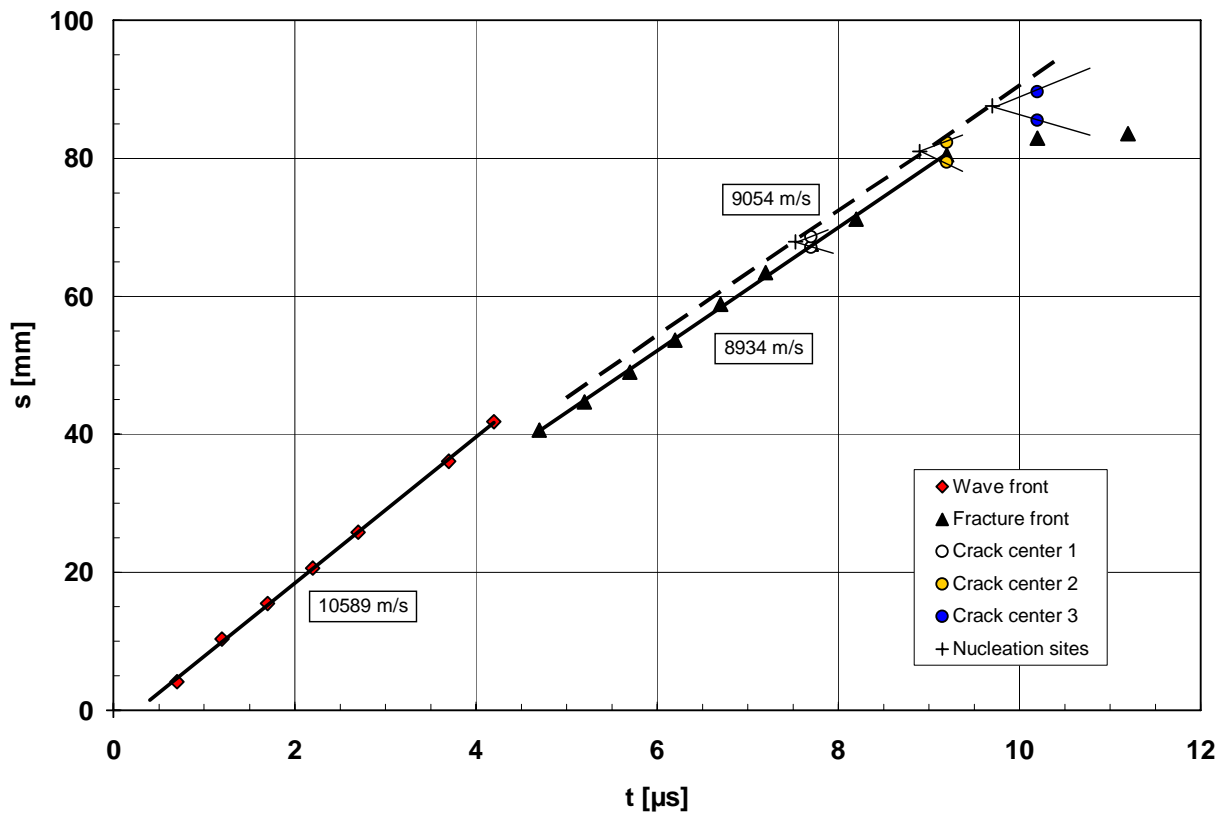

Fig. 9:   Path-time data of wave and fracture propagation in inhomogeneous specimen (internal stress), impacted at 390 m/s.

One AlON specimen of 10 mm thickness contained a flaw that was visible to the naked eye. It was not possible to determine the nature of the flaw, but from its appearance it could be concluded that it was either a small bubble or inclusion in the interior of the tile. However, the flaw was not visible in the high-speed photographs. The specimen was also tested at an impact velocity of ≈ 400 m/s. Figure 10 shows a selection of eight photographs from this test. The complete series of photographs is presented in Figure A6 of the Appendix.
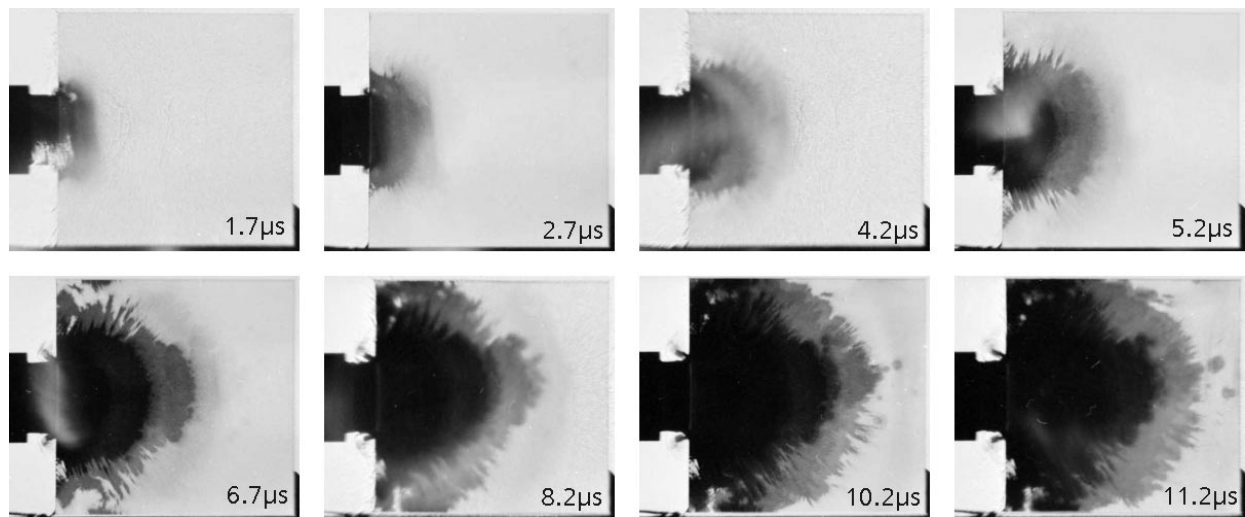

Fig. 10:   Selection of eight shadowgraphs from impact on inhomogeneous AlON specimen, Test No. 14924, v_p = 385 m/s.

From the view of the camera the position of the flaw was in the upper left quadrant of the specimen. It was expected that the flaw might act as a nucleation site for damage on the arrival of the stress wave. The photographs in Figure 10 demonstrate that this hypothesis could not be confirmed. The same phenomena as in test no. 14923 were observed and the coherent fracture front velocity of 8918 m/s was nearly equal to fracture front velocity determined in the previous test at 390 m/s. The time dependent progress of the wave and fracture front is illustrated in Figure 11. During the first six microseconds a wave front was observed which propagated at an average speed of 10594 m/s. Considering the crack centers ahead of the coherent fracture front, a damage velocity of 9145 m/s could be determined.
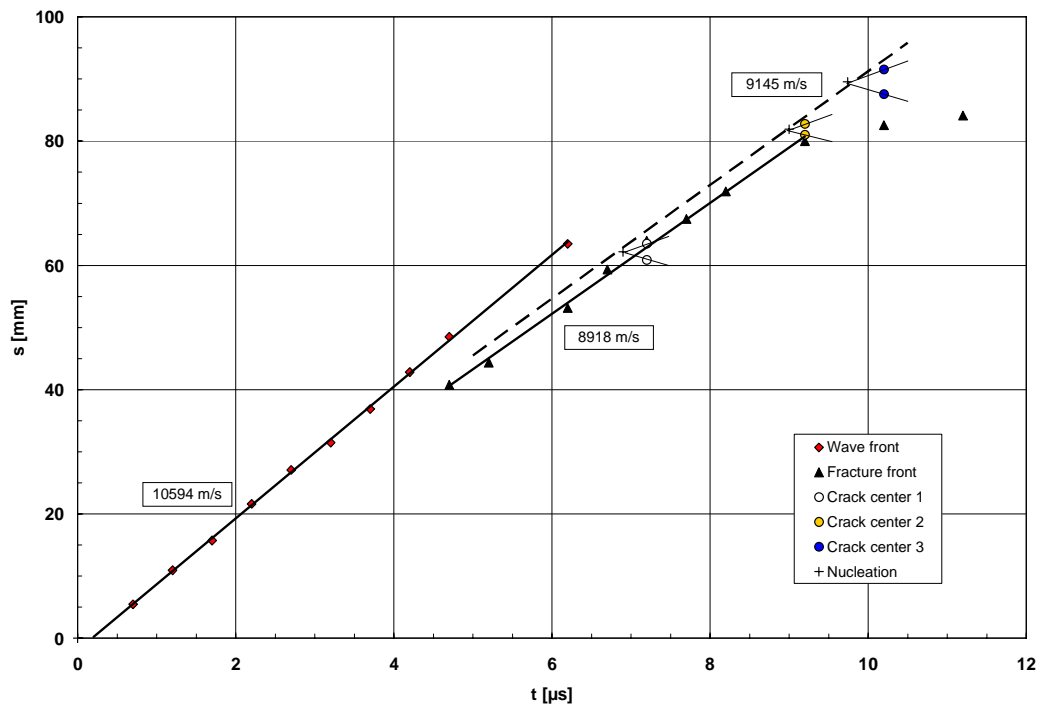
Fig. 11:   Path-time data of wave and fracture propagation in specimen with flaw, impacted at 385 m/s.

2.2.3 Test with specimen of 25 mm thickness

In order to test the influence of specimen thickness on damage formation one experiment was conducted with a specimen of 25 mm thickness. The specimen also exhibited the kind of inhomogeneity as described with the specimen of test no. 14923 (see Fig. 7). Figure 12 shows a selection of eight photographs from this test. The complete series of photographs is presented in Figure A7 of the Appendix.

The photographs of Figure 12 illustrate that the same phenomena occur in the thick specimen as were observed in the 10 mm specimens. The most advanced front that could be recognized propagated at an average velocity of 10478 m/s, and thus was identified as a longitudinal wave. Compared to the 10 mm specimens, the wave front was much better discernible in the thick specimen. In contrast to the wave front, the tip of the fracture front was hardly discernible in most of the photographs. Only three photographs allowed an accurate measurement of the fracture front position. The average velocity determined from these data was 8256 m/s.
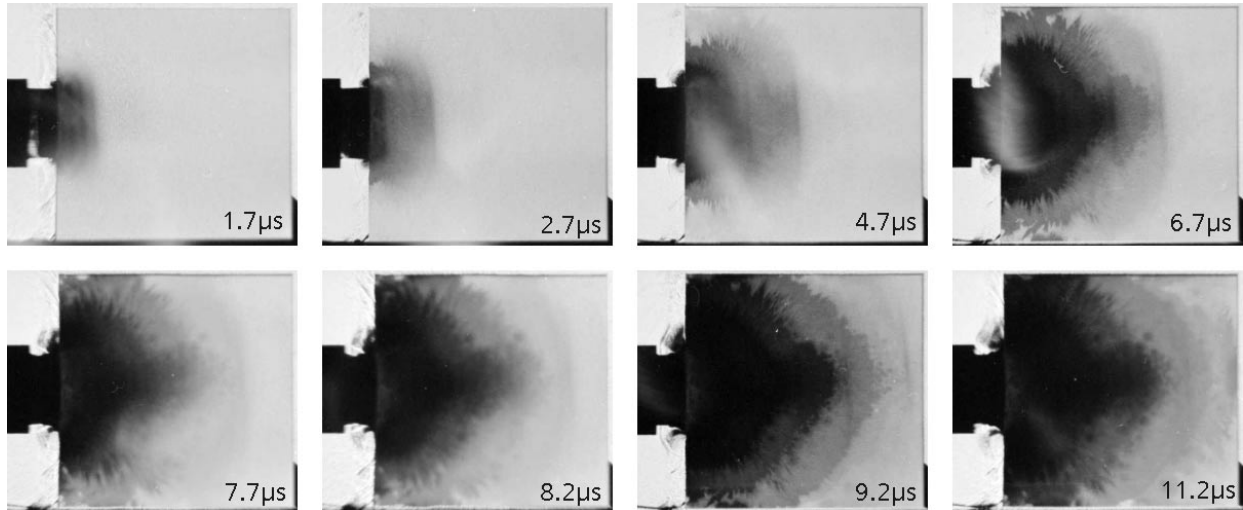
Fig. 12:   Selection of eight shadowgraphs from impact on AlON specimen of 25 mm thickness, Test No. 14925, v_p = 385 m/s.

The path-time histories of the wave and fracture front are depicted in Figure 13. The blurred appearance of the fracture front is attributed to the enhanced scatter of light, due to the higher thickness of the specimen on one hand. On the other hand, the effect of birefringence shift is stronger with the thicker specimen.
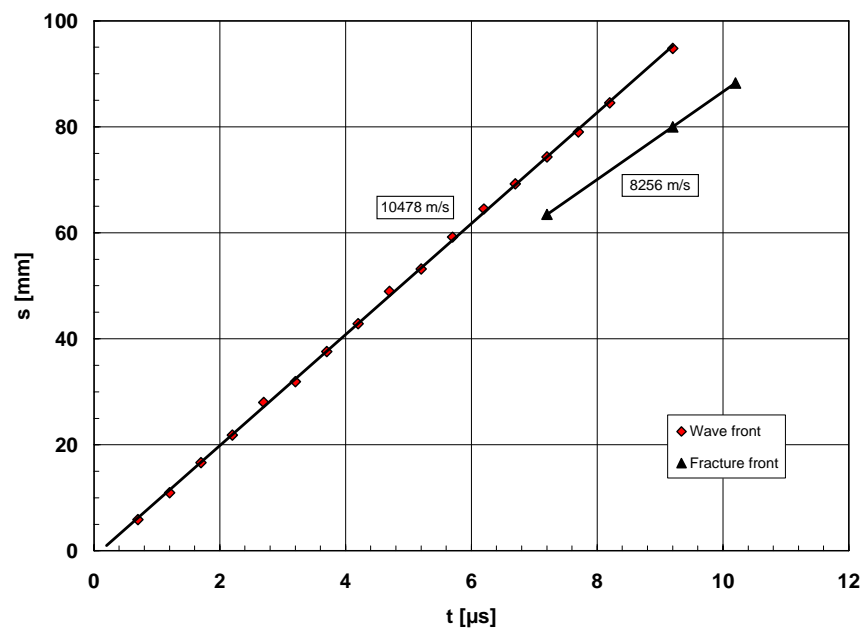

Fig. 13:   Path-time data of wave and fracture propagation in specimen of 25 mm thickness, impacted at 385 m/s.

2.2.4 Summary of results with AlON

A compilation of the measured stress wave, coherent fracture front and damage velocities is given in Table 4. The coherent fracture front velocities were all in the range from 8000 m/s to 9400 m/s, whereas the damage velocities ranged from 8900 m/s to 9800 m/s. The damage velocities are presented as a function of impact velocity in Figure 14 along with the data of other types of armor ceramics.

Table 4: Compilation of wave and fracture velocity data with AlON.

Test No.	Impact Vel. [m/s]	Optical Set-up	Stress Wave Velocity [m/s]	Coh. Fracture Front Velocity [m/s]	Damage Velocity [m/s]
14894	278	Shadowgraph	---	7994/8081	9066
14895	270	Cr. Polarizers	9944	---	---
14897	381	Shadowgraph	---	8381	9156
14898	368	Cr. Polarizers	9367	---	---
14906	820	Shadowgraph	---	8204	9145
14907	925	Cr. Polarizers	10438/9315	---	---
14908	588	Shadowgraph	---	8413	8976
14909	664	Cr. Polarizers	8968/10925	---	---
14923	390	Shadowgraph	10589	8934	9054
14924	385	Shadowgraph	10594	8918	9145
14925	385	Shadowgraph	10478	8256	---
14940	397	Reflected light	10564	9361	9767

In each of the ceramics the damage velocity increases with rising impact velocity. The damage velocities approach the longitudinal wave velocity c_L at high loadings. With most of the materials a steep rise of v_D is observed in the range of impact velocities between 150 m/s and 200 m/s. Since all tests with AlON were conducted at impact velocities above 250 m/s high damage velocities had been expected. The damage velocities were all in the range from 85 % to 95 % of the longitudinal wave velocity, which corresponds to the results with aluminum oxide.
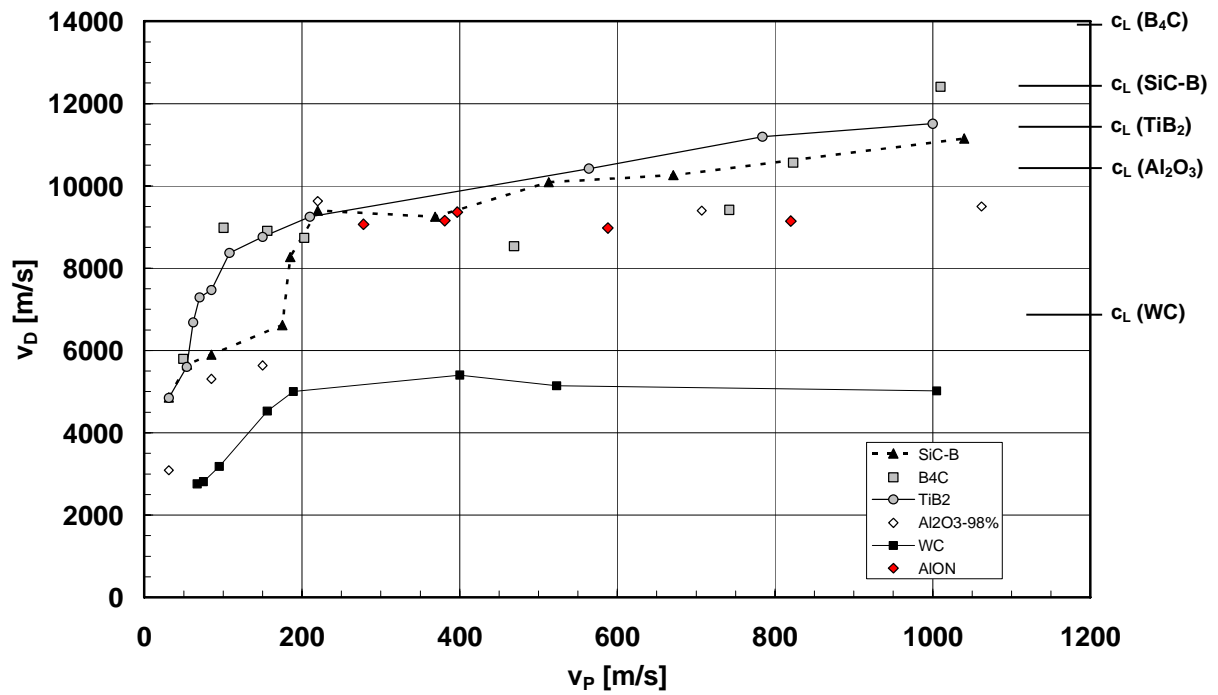
Fig. 14: Damage velocity v_D versus impact velocity v_P for different armor ceramics.

3   Conclusion

– The edge-on impact technique was modified in order to visualize stress wave propagation in transparent ceramics. The specimens were placed between crossed polarizers and the photo-elastic effect was successfully utilized to visualize the stress waves.

– Pairs of impact tests at approximately equivalent velocities were carried out in transmitted plain (shadowgraphs, visualization of damage) and crossed polarized light (visualization of wave propagation).

– The experiments provided direct evidence of ceramic damage by nucleation and growth of fracture initiated by the stress waves, ahead of the coherent fracture front growing from the impacted edge.

– A comparison of the results in a reflected light set-up and the shadowgraphs indicated fracture nucleation in the interior of the ceramic.

– The experimental results provide a data basis for a deeper analysis of the damage mechanisms by means of numerical simulation.

4   References

[1]   Senf, H., Straßburger, E., Rothenhäusler, H., "Stress wave induced damage and fracture in impacted glasses", J. PHYS. IV, C8, Vol. 4, pp. 741-746, 1994.

[2]   Senf, H., Straßburger, E., Rothenhäusler, "Visualization of fracture nucleation during impact in glass", Metallurgical and Materials Applications of Shock-Wave and High-Strain-Rate Phenomena, pp. 163-170, 1995.

[3]   E. Straßburger: "Visualization of Impact Damage in Ceramics Using the Edge-On Impact Technique"; Int. Journal of Applied Ceramic Technology, Topical Focus: Ceramic Armor, The American Ceramics Society, Vol. 1, Number 3, pp. 235-242, 2004

[4]   Senf, H., Straßburger, E., Rothenhäusler, "A Study of Damage during Impact in Zerodur", J. PHYS IV, C3, Vol. 7, pp. 1015-1020, 1997.

[5]   Patel, P. J., Gilde, G. A., "Transparent Armor Materials: Needs and Requirements"; Ceramic Transactions Vol. 134, pp. 573-586, 2001.

[6]   E. Straßburger: "High-Speed Photographic Study of Wave Propagation and Impact Damage in Transparent Aluminum Oxynitride (AlON)"; 1st Interim Report, Contract No. N62558-04-P-6031, EMI Report E 29/04, November 2004

[7]   E. Straßburger: "High-Speed Photographic Study of Wave Propagation and Impact Damage in Transparent Aluminum Oxynitride (AlON)"; 2nd Interim Report, Contract No. N62558-04-P-6031, EMI Report E 11/05, March 2005

[8]   Straßburger, E., Patel, P., McCauley, J.W., Templeton, D.W., "High-Speed Photographic Study of Wave and Fracture Propagation in Fused Silica", Proc. 22nd Int. Symp. on Ballistics, 14-18 Nov., Vancouver, BC, Canada, 2005

[9]   H. Vollkommer: "Schlierenoptische Untersuchung des Schneidenstoßes auf eine Plattenkante", Ernst-Mach-Institut, EMI-Report 1/67, 1967

[10]   G.S. Settles: "Schlieren and Shadowgraph Techniques: visualizing phenomena in transparent media", Springer, Heidelberg, 2001

[11]   J. Beinert, „Schlierenoptische Untersuchungen zur Ausbreitung kurzer elastischer Impulse in Platten", PhD Thesis, Fraunhofer-Institute for Mechanics of Materials, Freiburg, Germany, 1974

[12]   E. Straßburger, H. Senf, "Experimental Investigations of Wave and Fracture Phenomena in Impacted Ceramics and Glasses", U.S. Army Research Laboratory contractor report ARL-CR-214, 1995; re-publication of EMI-Report 3/94

[13]   Straßburger, E., Patel, P., McCauley, J.W., Templeton, D.W., "Visualization of Wave Propagation and Impact Damage in a Polycrystalline Transparent Ceramic – AlON", Proc. 22nd Int. Symp. on Ballistics, 14-18 Nov., Vancouver, BC, Canada, 2005
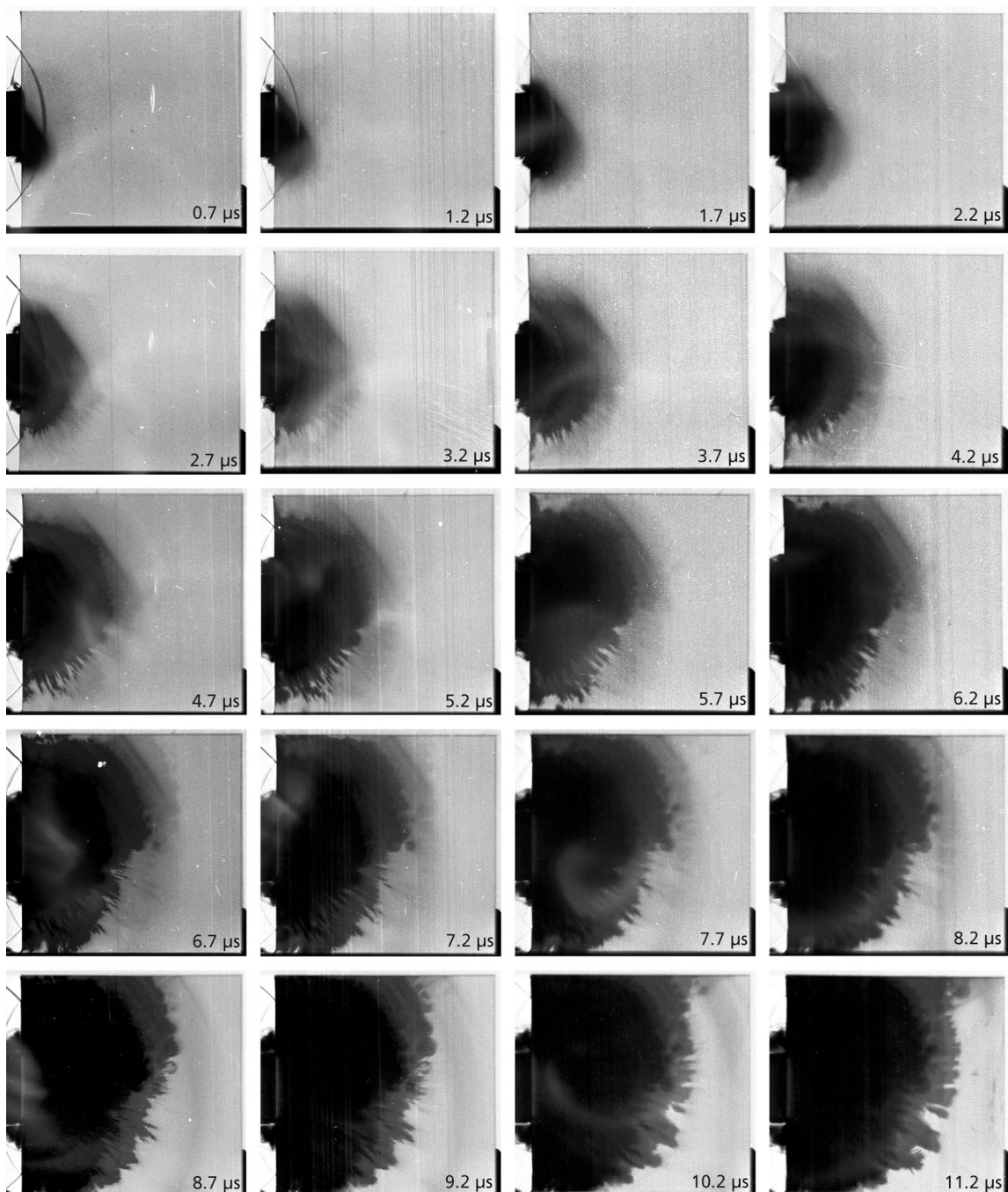
5   Appendix

Fig. A1:   High-Speed Photographs: Shadowgraph Arrangement, Positive Patterns, Side View
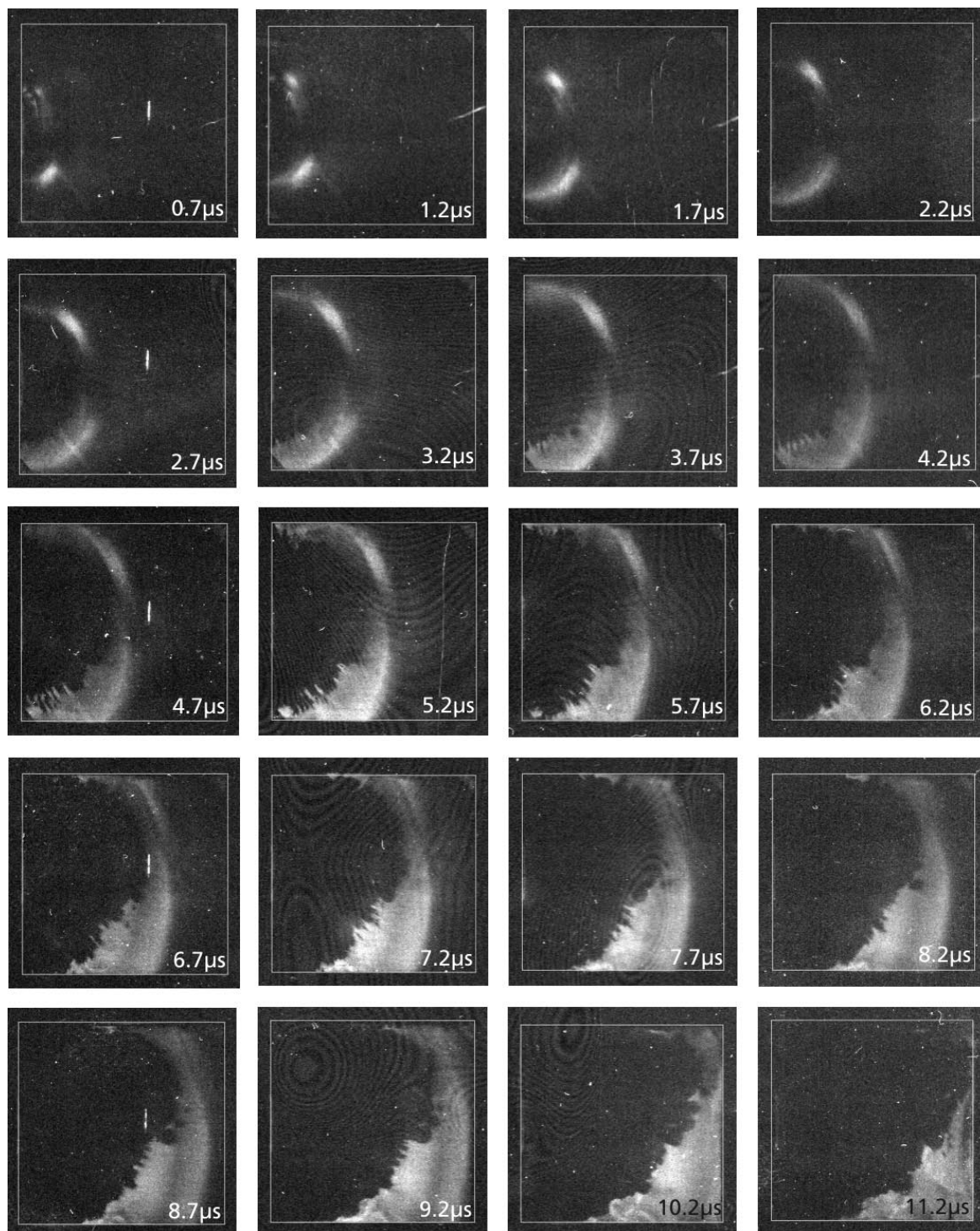Test No. 14906, $v_P = 820$ m/s.

Fig. A2: High-Speed Photographs: Crossed Polarizers Arrangement, Positive Patterns, Side View
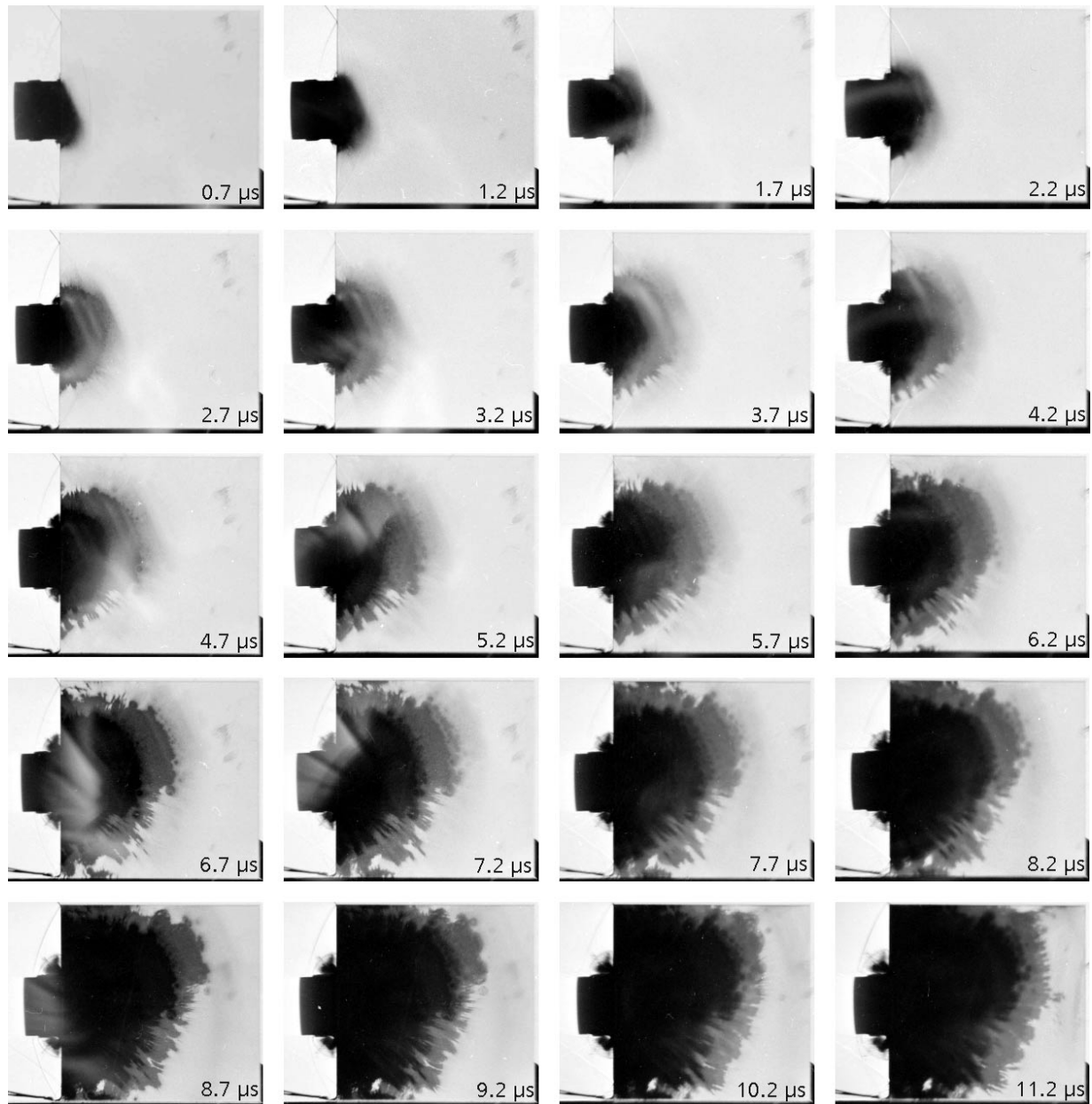Test No. 14907, $v_P = 925$ m/s.

Fig. A3:   High-Speed Photographs: Shadowgraph Arrangement, Positive Patterns, Side View
Test No. 14908, v_P = 588 m/s.

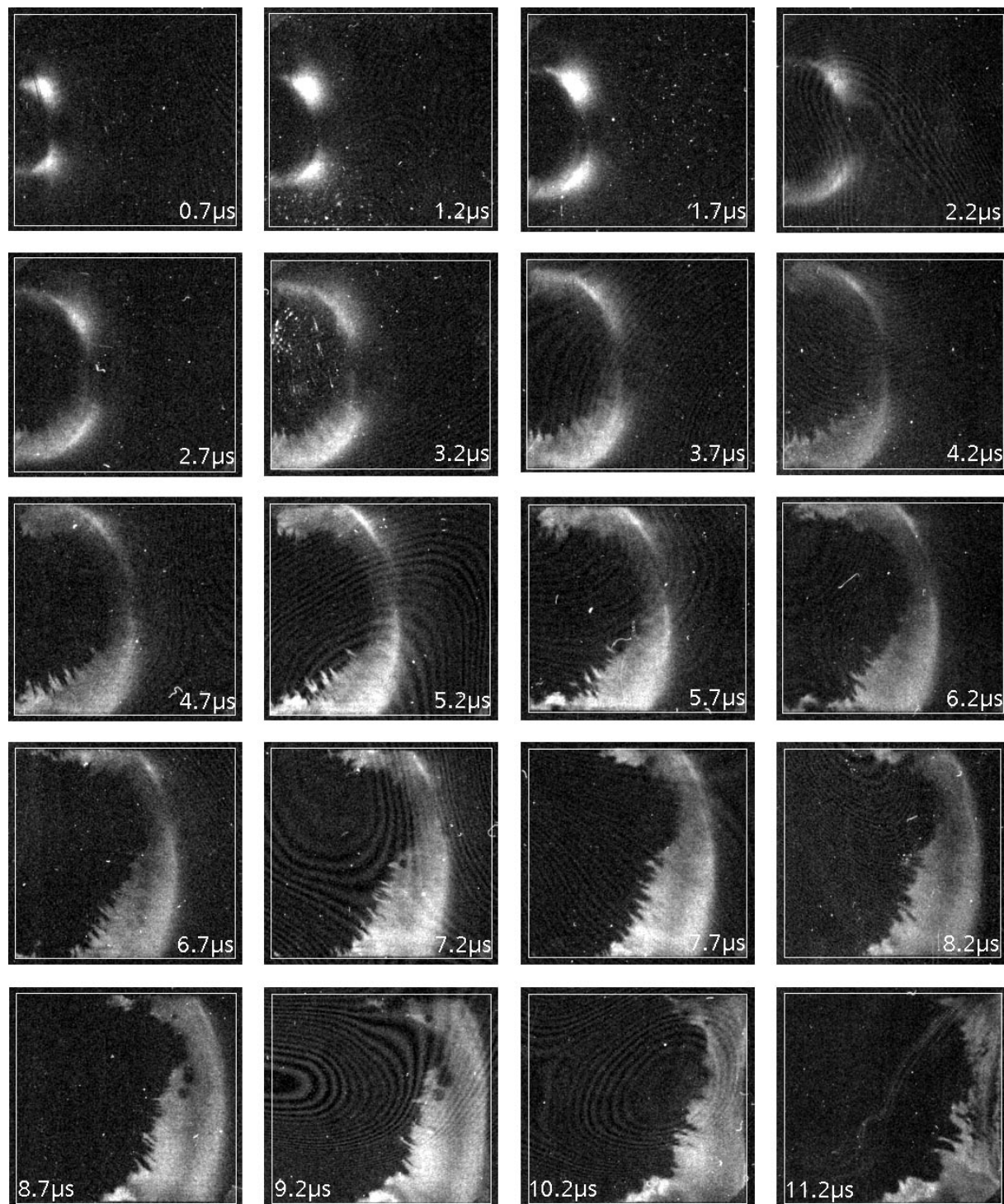Fig. A4: High-Speed Photographs: Crossed Polarizers Arrangement, Positive Patterns, Side View
Test No. 14909, $v_P = 664$ m/s.

Fig. A5: High-Speed Photographs: Shadowgraph Arrangement, Positive Patterns, Side View
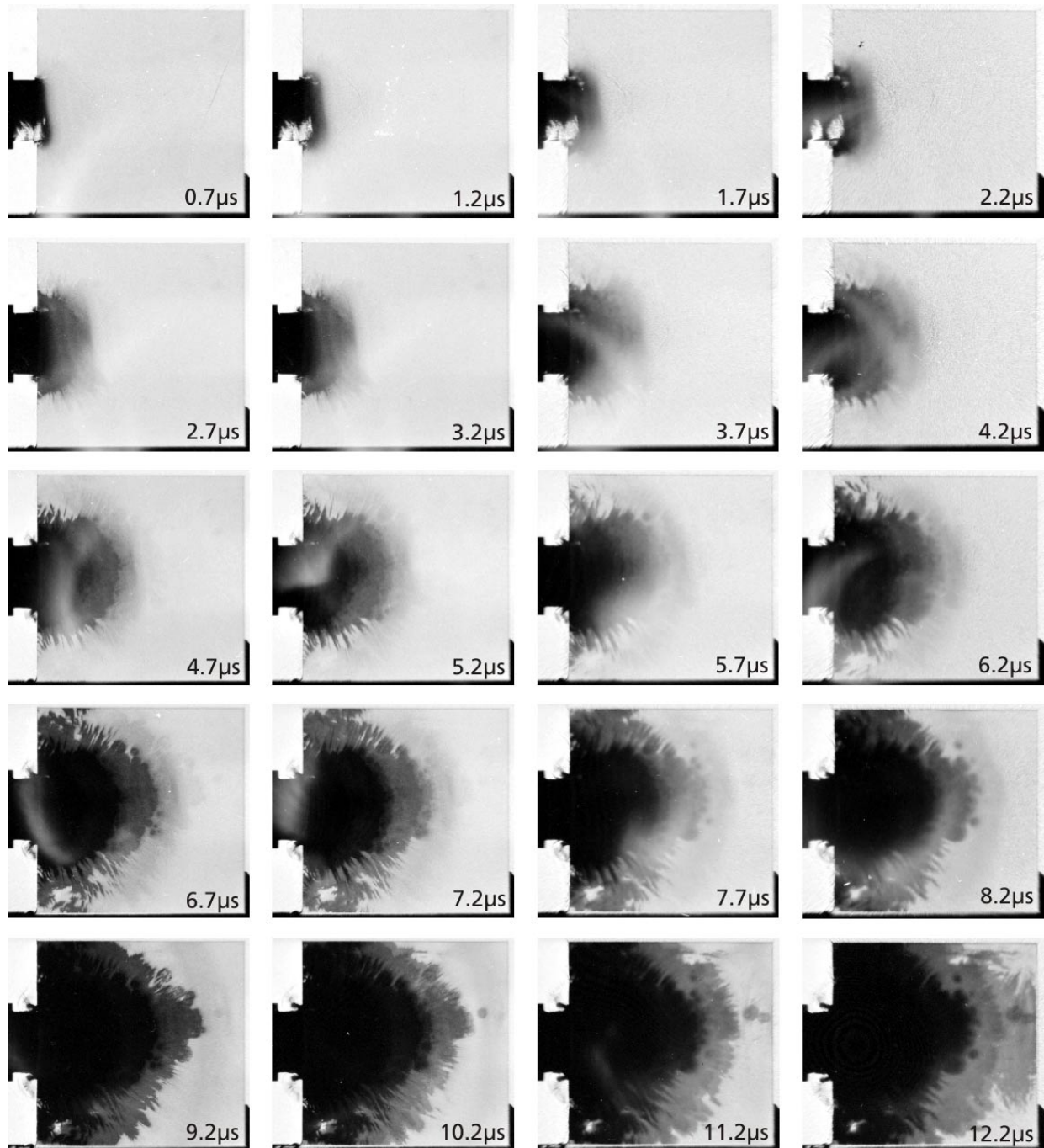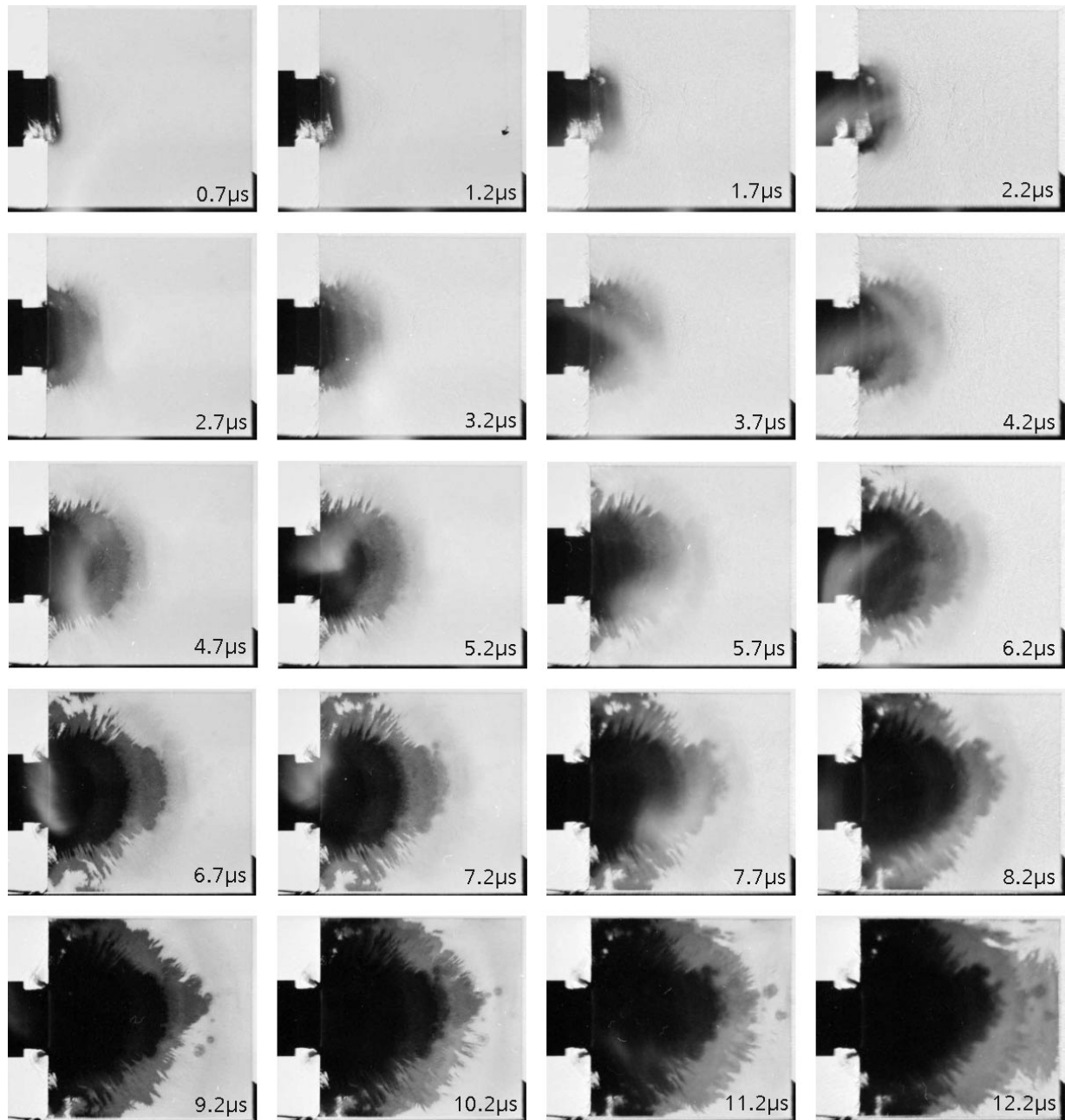inhomogeneous specimen; Test No. 14923, v_P = 390 m/s.

Fig. A6:   High-Speed Photographs: Shadowgraph Arrangement, Positive Patterns, Side View specimen with flaw; Test No. 14924, $v_p = 385$ m/s.
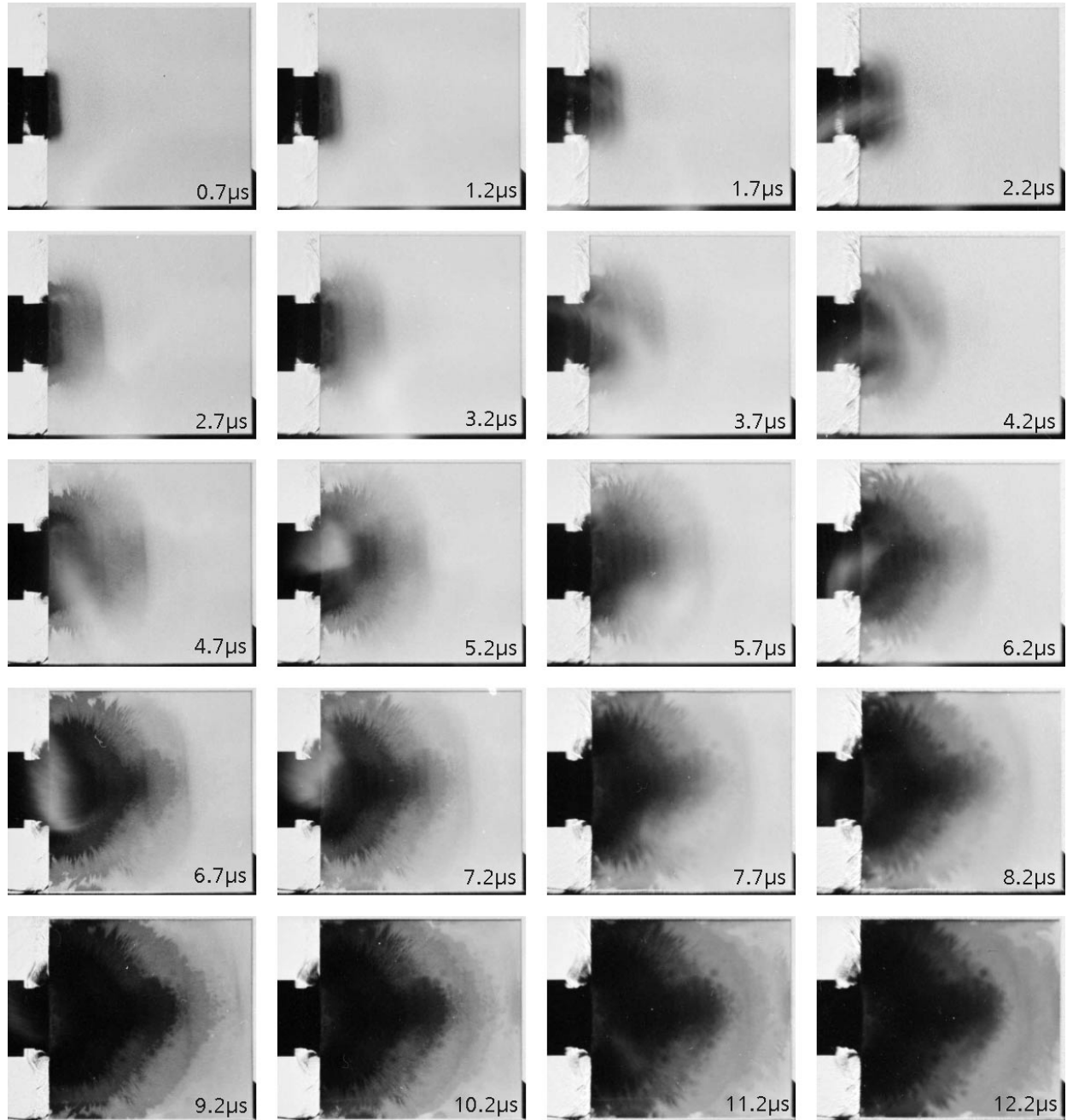
Fig. A7:   High-Speed Photographs: Shadowgraph Arrangement, Positive Patterns, Side View
specimen of 25 mm thickness; Test No. 14925, $v_P = 385$ m/s.

List of Distribution

Report No. E 08/06   **Copies: 10 + 1**

Author: E. Straßburger
Title: High-Speed Photographic Study of Wave Propagation and Impact
                     Damage in Transparent Aluminum Oxynitride (ALON): Final Report

Internal Distribution:
Author(s):   E. Straßburger
                     M. Salk, M. Steinhauser
                     K. Thoma

EMI Freiburg   1
EMI Efringen-Kirchen   1

ARL-European Research Office
ERO Program Assistant, Edison House   1 (**PDF** by e-mail)
223 Old Marylebone Road, London, NW1 5TH, England
ERO_PROGRAMS@USARDSGUK.ARMY.MIL

U.S. Army Research Laboratory   1
James McCauley, Attn: AMSRL-WM-M
Rodman Materials Research Laboratory, Bldg. 4600
Aberdeen Proving Ground, MD 21005-5066, USA

Parimal Patel, Attn: AMSRD-ARL-WM-MD   1
Aberdeen Proving Ground, MD 21005-5066, USA

W. A. Gooch, Attn: AMSRL-WT-TA   1
Aberdeen Proving Ground, MD 21005-5066, USA

U.S. Army TARDEC   1
Douglas W. Templeton, U.S. Army TARDEC
Warren, MI 48397-5000, USA

REPORT DOCUMENTATION PAGE		*Form Approved* *OMB No. 0704-0188*

Public reporting burden for this collection of information is estimated to average 1 hour per response, including the time for reviewing instructions, searching existing data sources, gathering and maintaining the data needed, and completing and reviewing this collection of information. Send comments regarding this burden estimate or any other aspect of this collection of information, including suggestions for reducing this burden to Washington Headquarters Services, Directorate for Information Operations and Reports, 1215 Jefferson Davis Highway, Suite 1204, Arlington, VA 22202-4302, and to the Office of Management and Budget, Paperwork Reduction Project (0704-0188), Washington, DC 20503

1. AGENCY USE ONLY (Leave blank)	2. REPORT DATE 02/21/2006	3. REPORT TYPE AND DATES COVERED Final Report, 07/2004–07/2005	

4. TITLE AND SUBTITLE HIGH-SPEED PHOTOGRAPHIC STUDY OF WAVE PROPAGATION AND IMPACT DAMAGE IN TRANSPARENT ALUMINUM OXYNITRIDE (AlON)	5. FUNDING NUMBERS
6. AUTHOR(S) E. Straßburger	

7. PERFORMING ORGANIZATION NAME(S) AND ADDRESS(ES)	8. PERFORMING ORGANIZATION REPORT NUMBER
Fraunhofer-Gesellschaft e.V. Fraunhofer-Institut für Kurzzeitdynamik Hansastrasse 27 c Ernst-Mach-Institut D-80686 München Am Klingelberg 1 Germany D-79588 Efringen-Kirchen Germany	E 08/06 N62558-04-P-6031 R&D 9779-TA-01

9. SPONSORING / MONITORING AGENCY NAME(S) AND ADDRESS(ES)	10. SPONSORING / MONITORING AGENCY REPORT NUMBER
US Naval Regional Contracting Center, Det. London Government Buildings, Block 2, Wing 12 Lime Grove, Ruislip, Middlesex, HA4 8BX England	

11. SUPPLEMENTARY NOTES

12a. DISTRIBUTION / AVAILABILITY STATEMENT APPROVED FOR PUBLIC RELEASE: DISTRIBUTION UNLIMITED	12b. DISTRIBUTION CODE

13. ABSTRACT *(Maximum 200 Words)*

Fused silica and AlON specimens were tested by means of a modified Edge-On Impact technique. The specimens were placed between crossed polarizers and the photo-elastic effect was utilized to visualize the stress waves. Pairs of impact tests at approximately equivalent velocities were carried out in transmitted plain (shadowgraphs, visualization of damage) and crossed polarized light (visualization of wave propagation). The experiments provided direct evidence of ceramic damage by nucleation and growth of fracture initiated by the stress waves, ahead of the coherent fracture front growing from the impacted edge. A comparison of the results in a reflected light set-up and the shadowgraphs indicated fracture nucleation in the interior of the ceramic. The experimental results provide a data basis for a deeper analysis of the damage mechanisms by means of numerical simulation.

14. SUBJECT TERMS Edge-on impact test, visualization, fracture propagation, shadowgraph, ALON, fused silica, Cranz-Schardin camera, crossed polarizers configuration	15. NUMBER OF PAGES 33
	16. PRICE CODE

17. SECURITY CLASSIFICATION OF REPORT UNCLASSIFIED	18. SECURITY CLASSIFICATION OF THIS PAGE UNCLASSIFIED	19. SECURITY CLASSIFICATION OF ABSTRACT UNCLASSIFIED	20. LIMITATION OF ABSTRACT

NSN 7540-01-280-5500

Standard Form 298 (Rev. 2-89)
 Prescribed by ANSI Std. Z39-18
 298-102